Title

How important is thermal expansion for predicting molecular crystal structures and thermochemistry at finite temperatures?

Journal

Acta Crystallographica Section B: Structural Science, Crystal Engineering and Materials, 72(4)

ISSN

2052-5192

Authors

Heit, Yonaton N

Beran, Gregory JO

Publication Date

2016-08-01

DOI

10.1107/s2052520616005382

Peer reviewed

How important is thermal expansion for predicting molecular crystal structures and thermochemistry at finite temperatures?

Yonaton N. Heit and Gregory J. O. Beran*

Department of Chemistry, University of California, Riverside, California 92521, USA

E-mail: gregory.beran@ucr.edu

March 26, 2016

Abstract

Molecular crystals expand appreciably upon heating due to both zero-point and thermal vibrational motion, yet this expansion is often neglected in molecular crystal modeling studies. Here, a quasi-harmonic approximation is coupled with fragment-based hybrid many-body interaction calculations to predict thermal expansion and finite-temperature thermochemical properties in crystalline carbon dioxide, ice Ih, acetic acid, and imidazole. Fragment-based second-order Møller-Plesset perturbation theory (MP2) and coupled cluster theory with singles, doubles and perturbative triples (CCSD(T)) predict the thermal expansion and the temperature dependence of the enthalpies, entropies, and Gibbs free energies of sublimation in good agreement with experiment. The errors introduced by neglecting thermal expansion in the enthalpy and entropy cancel somewhat in the Gibbs free energy. The resulting ∼1–2 kJ/mol errors in the free energy near room temperature are comparable to or smaller than the

*To whom correspondence should be addressed

errors expected from the electronic structure treatment, but they may be sufficiently large to affect free energy rankings among energetically close polymorphs.

1 Introduction

Molecular crystals occur in pharmaceuticals, organic semiconductor materials, and many other areas of chemistry. The molecular packing in a crystal has substantial impacts on its properties. Polymorphism, or the tendency for a given molecule to adopt multiple distinct packing motifs, provides excellent examples of this phenomenon. Estimates suggest that at least half of organic crystals exhibit multiple polymorphs.[1] Undesirable pharmaceutical polymorphs can exhibit reduced bioavailability,[2–5] while at other times alternative crystal forms may be targeted for their improved physical properties.

Computational chemistry plays an increasingly important role in predicting crystal structures, phase diagrams, spectroscopic observables, mechanical properties, and other molecular crystal properties that can help characterize crystals or identify potential new forms. Particular attention in recent years has been focused on crystal structure prediction.[6–11] The most stable crystal structures exhibit the lowest free energies. However, rankings based on lattice energies, which neglect both thermal and vibrational zero-point energy effects, are often used as proxy for free energy. Twenty years ago, Gavezzotti and Filippini[12] argued that the free energy contributions arising from room-temperature lattice vibrational entropy are generally smaller than the enthalpic differences between polymorphs.

More recently, Nyman and Day[13] surveyed 508 sets of polymorphic crystals and found that the harmonic vibrational free energy contributions at 300 K often contribute $\sim$1 kJ/mol or less to the relative stabilities among polymorphs. Though the vibrational free energy contribution is small, they observed that it frequently opposes the lattice energy difference, which suggests that it will eventually lead to an enantiotropic phase transition at some temperature (unless the crystal melts first). Indeed, in almost 10% of the cases they considered,

free energy rankings at room temperature predict a different polymorph stability than the one inferred from the lattice energy. Such observations are consistent with the frequency with which temperature-dependent transitions between polymorphs occur experimentally.

Many examples where vibrational zero-point and free energy contributions feature in the context of polymorphism can be found in the literature, including glycol and glycerol,[14] pyridine,[15] glycine,[16] co-crystals of urea and acetic acid,[17] and aspirin.[18] In aspirin, for instance, the two polymorphs are predicted to be virtually degenerate in lattice energy, but the free energy appears to favor form I.[18] A couple of groups considered the impact of free energy ranking in the fourth blind test of crystal structure prediction, though the free energy contributions did not significantly revise the lattice energy rankings in those particular crystals.[9]

Temperature also plays an important dynamical role in molecular crystals. Thermal averaging over lattice energy minima often effectively reduces the number of minima on the free energy surface.[19] Metadynamics studies on benzene,[20] 5-fluorouracil,[21] and pigment red 179[22] each demonstrate a reduction from many lattice energy minima to a smaller number of free energy minima, though the extent of reduction varies widely with the nature of the system.[19]

Finite temperature effects on crystal properties are not limited to thermochemistry. For example, crystals typically expand upon heating, which affects the electronic coupling and non-local electron-phonon coupling in organic semi-conductors. Shifting the intermolecular separation between two adjacent anthracene molecules taken from the crystal can alter the transfer integral by $\sim$30%, for example.[23] Thermal expansion also narrows the valence and conduction bandwidths in organic semiconductor materials like pentacene and rubrene.[24]

All of these examples demonstrate the potential importance of accounting for finite temperature and computing free energies instead of lattice energies when modeling molecular crystals. However, even studies that do estimate finite-temperature free energies often do so using a fixed-cell harmonic approximation based on the minimum electronic energy struc-

ture, ignoring thermal expansion of the crystal. This is especially true when the molecular crystals are modeled using computationally expensive electronic structure methods instead of classical force fields. Thermal expansion alters many crystal properties. For example, expansion-induced softening of the low-frequency intermolecular lattice phonon modes will increase the magnitude of the entropic contributions. This raises the question: How significant are thermal expansion effects in predicting molecular crystal properties at finite temperatures?

Modeling thermal expansion requires minimizing the crystal structure at a given temperature with respect to the free energy instead of the more readily computed electronic energy. Doing so using conventional molecular dynamics and/or free energy sampling techniques is generally computationally prohibitive when using quantum mechanical techniques. Instead, the quasi-harmonic approximation provides a computationally practical alternative to free energy sampling techniques.[25–27] It assumes that anharmonicity in the crystal arises primarily from the intermolecular expansion and approximates the vibrational free-energy contributions as a function of unit cell volume.

Despite its simplicity, the quasi-harmonic approximation provides a useful tool for investigating how the unit cell volume and other properties of small-molecule crystals vary as a function of temperature (though it does not address the dynamical thermal averaging aspects mentioned earlier). In a recent study on crystalline carbon dioxide (phase I),[28] we demonstrated that a quasi-harmonic treatment of thermal expansion at the complete-basis-set (CBS) limit second-order Møller-Plesset perturbation theory (MP2) or even coupled cluster singles, doubles, and perturbative triples (CCSD(T)) level of theory accurately captures the $\sim$10% volume expansion that occurs between the minimum electronic energy structure and the structure near the 194.7 K sublimation point. The same model also allows one to predict the sublimation enthalpy and entropy and the room-temperature bulk modulus in excellent agreement with experiment. In contrast, neglecting thermal expansion introduces appreciable errors in the predicted thermochemistry and mechanical properties.

These high-level calculations in a periodic crystal are made feasible using the fragment-based hybrid many-body interaction (HMBI) model,[29–31] which combines a QM treatment of the intra- and dominant intermolecular interactions with a classical molecular mechanics (MM) treatment of the weaker interactions.

Here, we extend the previous study by comparing predictions of finite-temperature properties in several different small-molecule crystals: carbon dioxide, ice Ih, the orthorhombic polymorph of acetic acid, and the α polymorph of imidazole. These relatively simple crystals were chosen because they exhibit a variety of intermolecular packing interactions, they have a experimental data available at various different temperatures, and they are small enough to enable relatively high-level electronic structure methods to be employed. The absence of appreciable conformational flexibility in these small molecules provides a best-case scenario for the quasi-harmonic approximation, since any changes in the intramolecular structures with temperature will be small.

In the following sections, we first examine the extent of thermal expansion that occurs in each crystal due to zero-point and thermal contributions. The degree of expansion observed varies with the types of intermolecular interactions found in the different crystals. Second, we evaluate the performance of fragment-based electronic structure models with and without quasi-harmonic expansion for predicting the enthalpies, entropies, and Gibbs free energies of sublimation for these crystals over a range of temperatures. The predictions are assessed against experimental data or empirical results derived from experiment. Finally, we investigate the importance of electronic structure method and basis set on predicting these properties correctly, and we attempt to decouple effects of the model chemistry on the structure optimization/phonon calculation from those on the lattice energy evaluation.

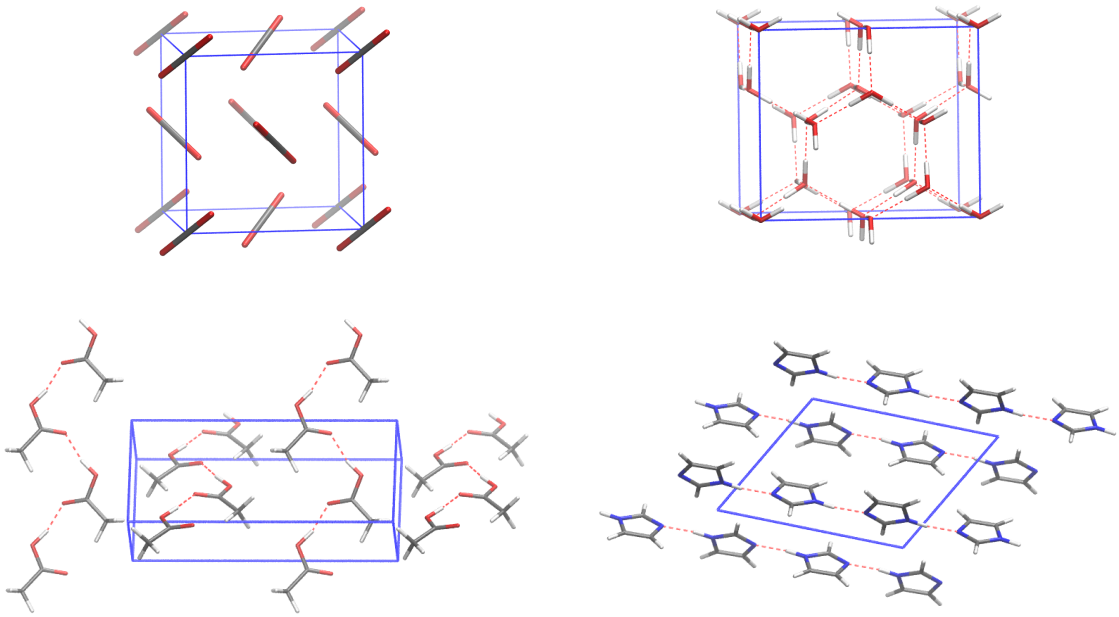

Figure 1: *Clockwise from top left:* Structures of phase I carbon dioxide, ice Ih, α imidazole, and orthorhombic acetic acid.

2 Theory

2.1 Quasi-harmonic structure optimization

The structure of a crystal at a given pressure and temperature is determined by minimizing the Gibbs free energy,

$$G(T,P) = U_{el} + PV + F_{vib}(T) \tag{1}$$

with respect to the atomic coordinates and unit cell lattice parameters. In this equation, U_{el} is the internal (electronic) energy, PV is the pressure/volume contribution, and F_{vib} is the Helmholtz vibrational free energy.

The electronic energy U_{el} is determined using the fragment-based hybrid many-body interaction (HMBI) model.[32–35] The HMBI model combines a QM treatment of the individual molecules in the unit cell (1-body terms) and their short-ranged pairwise interactions (SR 2-body terms) with an MM polarizable force field treatment of longer-range (LR 2-body

terms) and many-body intermolecular interactions,

$$U_{el} = E^{\mathrm{QM}}_{\text{1-body}} + E^{\mathrm{QM}}_{\text{SR 2-body}} + E^{\mathrm{MM}}_{\text{LR 2-body}} + E^{\mathrm{MM}}_{\text{many-body}} \tag{2}$$

In practice, the short-range two-body QM terms capture interactions between molecules inside the unit cell and the nearby periodic image cells, while the long-range two-body MM terms are handled via Ewald summation.

The Helmholtz vibrational free energy $F_{vib}(T)$ is derived from standard harmonic oscillator vibrational partition function expressions obtained from statistical mechanics. It includes both zero-point energy and thermal contributions to the free energy:

$$F_{vib}(T) = \frac{N_a}{k_{total}} \sum_{k}^{k_{total}} \sum_{i} \frac{\hbar\omega_{k,i}}{2} + k_B T \ln\left[1 - \exp\left(-\frac{\hbar\omega_{k,i}}{k_B T}\right)\right] \tag{3}$$

where k_{total} the total number of k-points. Evaluating $F_{vib}(T)$ requires knowledge of the harmonic vibrational frequencies for the current unit cell. In principle, this requires optimizing the atomic positions with fixed lattice parameters followed by computing the phonon frequencies via lattice dynamics. Unfortunately, that repeating that process for each step in a free-energy minimization is very computationally demanding.

Instead, the Gibbs free energies are estimated using the quasi-harmonic approximation. Many versions of the quasi-harmonic approximation exist,[27,36,37] but one frequently employs a statically constrained approximation[38] in which only the cell volume directly depends on the temperature and pressure. The atomic coordinates within the unit cell are obtained by minimizing the internal (electronic) energy for a given unit cell volume.

In the simplest case, the cell volume may be set to match experimentally known lattice parameters at an appropriate temperature.[39,40] More generally, a scan can be performed over a series of volumes. At each volume, one optimizes the atomic coordinates, computes the phonon frequencies, and then computes the free energy. A free-energy minimization is then performed by fitting the set free-energies obtained in this manner to some functional form

or by performing some other interpolation scheme.[26,41–43]

However, scanning the free energy surface in this manner still requires performing phonon calculations at many different volumes, which can be computationally demanding. An alternative, more computationally efficient approach which we adopt here evaluates mode-specific Grüneisen parameters that approximate how individual phonon frequencies vary with volume. This approach requires only a handful of expensive harmonic phonon calculations. This latter approach has been used with both classical mechanical force fields[44] and DFT[45] to study ices, for example.

In the mode-specific Grüneisen model used here, the i-th vibrational frequency $\omega_{k,i}$ at a particular unit cell volume V and k-point k is estimated relative to a reference harmonic frequency $\omega_{k,i}^{ref}$ computed at a reference unit cell volume V_{ref} according to the quasi-harmonic approximation. The quasi-harmonic approximation defines the change of the i-th vibrational frequency with respect to unit cell volume according to a mode-specific Grüneisen parameter $\gamma_{k,i}$,

$$\gamma_{k,i} = \frac{\partial \omega_{k,i}}{\partial V} \tag{4}$$

Integrating Eq 4 gives,

$$\omega_{k,i} = \omega_{k,i}^{ref} \left(\frac{V}{V^{ref}} \right)^{-\gamma_{k,i}} \tag{5}$$

Here, the reference volume and frequencies are obtained via optimizing the crystal unit cell with respect to the electronic energy U_{el}. The mode-specific Grüneisen parameters are determined via finite difference, using two additional structure optimizations and vibrational frequency calculations performed in fixed unit cells that have been expanded or compressed by a small amount.

The vibrational modes computed for a particular unit correspond to the zone-center ($\mathbf{k} = 0$) phonons. However, phonon dispersion at $\mathbf{k} \neq 0$ can play an important role. The phonon modes at a given k-point are evaluated via lattice dynamics,[46] which involves the

construction and diagonalization of the mass-weighted supercell dynamical matrix,

$$\hat{D}_{\alpha,\beta}(l,l',\mathbf{k}) = \frac{1}{\sqrt{M_l M_{l'}}} \sum_{\kappa} \frac{\partial V}{\partial R_\alpha(0)\partial R_\beta(\kappa)} \exp\left(-2\pi i \mathbf{k}\cdot\delta\mathbf{R}_{l,l'}(0,\kappa)\right) \tag{6}$$

where $\frac{\partial V}{\partial R_\alpha(0)\partial R_\beta(\kappa)}$ is an element of the supercell Hessian between coordinate $\alpha(0)$ of atom l in the central unit cell and coordinate $\beta(\kappa)$ of atom l' in periodic image cell κ. $\delta\mathbf{R}_{l,l'}(0,\kappa)$ is the distance between atom l and l'.

A major advantage a fragment-based methods like HMBI or the binary interaction model[47] have over more traditional models like periodic DFT or periodic MP2 is that the construction of the lattice dynamics supercell Hessian requires little additional computational cost compared to the standard unit cell Hessian. For HMBI, all the necessary QM contributions to the supercell Hessian are already available in the standard unit cell Hessian. The Hessian contributions arising from a monomer or a short range dimer two-body interactions in the standard Hessian can be transposed onto the translationally equivalent dimer in the supercell Hessian according to the periodic symmetry of the lattice. The only additional HMBI contribution needed is the MM supercell Hessian, which requires minimal additional computational effort compared to the cost of evaluating the QM two-body Hessian contributions.

2.2 Thermochemistry

Once the crystal structures and vibrational frequencies are known at a given temperature and pressure, one can compute other thermodynamic quantities. Here, we predict enthalpies, entropies, and Gibbs free energies of sublimation for comparison with experiment. These are computed as the enthalpy, entropy, or free energy difference between the gas and solid, with the solid contribution normalized according to the number of molecules n in the unit cell:

$$\Delta H_{sub} = H_{gas} - \frac{1}{n} H_{solid} \tag{7}$$

$$\Delta S_{sub} = S_{gas} - \frac{1}{n} S_{solid} \tag{8}$$

$$\Delta G_{sub} = H_{sub} - T\Delta S_{sub} \tag{9}$$

The enthalpy of the solid is computed from the electronic energy plus the PV term and the vibrational energy U_{vib}

$$H_{solid} = U_{el,solid} + PV + U_{vib,solid} \tag{10}$$

The harmonic vibrational energy is determined from the standard vibrational statistical mechanics equation,

$$U_{vib,solid} = \frac{N_A}{k_{total}} \sum_{k}^{k_{total}} \sum_{i} \left(\frac{\hbar\omega_{k,i}}{2} + \frac{\hbar\omega_{k,i}}{\exp\left(\frac{\hbar\omega_{k,i}}{k_B T}\right) - 1} \right) \tag{11}$$

The entropy of the solid is determined from its standard vibrational statistical mechanics equation plus the configurational entropy

$$S_{solid} = S_{solid,vib} + S_{conf} \tag{12}$$

$$S_{solid,vib} = \frac{N_A}{k_{total}} \sum_{k}^{k_{total}} \sum_{i} \left(\frac{\hbar\omega_{k,i}}{T\left(\exp\left(\frac{\hbar\omega_{k,i}}{k_B T}\right) - 1\right)} - k_B \ln\left[1 - \exp\left(-\frac{\hbar\omega_{k,i}}{k_B T}\right)\right] \right) \tag{13}$$

For most crystals considered here, the configurational entropy S_{conf} is set to zero. However, the intrinsic proton disorder in ice Ih produces a non-zero configurational entropy of $R \ln\left(\frac{3}{2}\right)$ according to the Pauling model.[48]

The gas phase is modeled as an ideal gas, with the enthalpy written as the sum of the electronic energy, the translational and rotational, and vibrational energy plus a factor of RT from the PV term.

$$H_{gas} = U_{el,gas} + U_{trans,gas} + U_{rot,gas} + U_{vib,gas} + RT \tag{14}$$

The translational energy ($U_{trans,gas}$) is equal to $\frac{3}{2}RT$. The rotational energy ($U_{trans,gas}$) is equal to RT for carbon dioxide (linear molecule) and $\frac{3}{2}RT$ for all other compounds considered here. The vibrational energy contribution ($U_{vib,gas}$) is given by,

$$U_{vib,gas} = N_A \sum_i \left(\frac{\hbar\omega_i}{2} + \frac{\hbar\omega_i}{\exp\left(\frac{\hbar\omega_i}{k_B T}\right) - 1} \right) \tag{15}$$

The gas phase entropy is the sum of the vibrational entropy ($S_{rot,gas}$), translation entropy($S_{trans,gas}$), the rotational entropy ($S_{rot,gas}$)

$$S_{gas} = S_{vib,gas} + S_{trans,gas} + S_{rot,gas} \tag{16}$$

Like the solid, the gas phase vibrational entropy is determined from the standard harmonic oscillator model,

$$S_{gas,vib} = N_A \sum_i \left(\frac{\hbar\omega_i}{T\left(\exp\left(\frac{\hbar\omega_i}{k_B T}\right) - 1\right)} - k_B \ln\left[1 - \exp\left(-\frac{\hbar\omega_i}{k_B T}\right)\right] \right) \tag{17}$$

The translation entropy is based on the ideal gas model,

$$S_{gas,tran} = R\ \ln\left[\left(\frac{2\pi M k_B T}{h^2}\right)^{\frac{3}{2}}\left(\frac{k_B T \exp\left(\frac{5}{2}\right)}{P}\right)\right] \tag{18}$$

The rotation of carbon dioxide is modeled as a linear ideal gas molecule,

$$S_{gas,rot,CO_2} = R\ \ln\left(\frac{8\pi^2 e T I k_B}{\sigma h^2}\right) \tag{19}$$

For all other molecules considered here, the rotational entropy was modeled according to the standard ideal gas rotational entropy expression for a non-linear polyatomic molecule,

$$S_{gas,rot} = R\ ln\left[\frac{(512\pi^7 T^3 e^3 k_B^3 I_A I_B I_C)^{\frac{1}{2}}}{\sigma h^3}\right] \tag{20}$$

where the I's are the moment of inertia. The number of symmetrical rotations (σ) is 2 for carbon dioxide and water and 1 for acetic acid and imidazole.

3 Computational Methods

Four crystals are considered here: ice Ih, carbon dioxide (phase I), acetic acid (ambient-pressure orthorhombic phase), and imidazole (α polymorph). The initial acetic acid and imidazole structures were taken from the Cambridge Structure Database (RefCodes ACETAC01[49] and IMAZOL06,[50] respectively). The initial ice structure used the dipole-free 16-molecule supercell obtained from Ref 51. All structures reported for carbon dioxide here were obtained previously[28] using the same quasi-harmonic techniques described here.

Electronic energies were calculated using the HMBI fragment approach. Substantial computational savings were achieved for acetic acid ($Pna2_1$ symmetry), imidazole ($P2_1/c$) and carbon dioxide ($Pa\bar{3}$) by exploiting space group symmetry for the energy, gradient, and Hessian evaluations.[52] Specific analysis of the symmetry for these crystals have been presented previously.[28,52] Ice exhibits $P1$ symmetry due to its disordered proton arrangement, which means that only basic translational symmetry arising from the periodic supercell can be exploited.

For structure optimizations and phonon frequency calculations, the QM contributions in HMBI were evaluated using the counterpoise-corrected[53] density-fitted MP2[54–57] and Dunning aug-cc-pVXZ (abbreviated to aXZ) basis sets[58,59] as implemented in Molpro 2012.[60,61] Molpro uses analytical MP2 nuclear gradients, while the Hessian elements were computed via finite difference of the gradients. Complete-basis-set (CBS) limit MP2 results were obtained using the standard two-point extrapolation models.[62,63] In some cases, calculations at the estimated CCSD(T)/CBS limit were also performed. For single-point energies or geometry optimizations, this was done using a focal point method which combined MP2/CBS results with a correction for the difference between MP2/aDZ and CCSD(T)/aDZ. For CCSD(T)-

level quasi-harmonic optimizations in carbon dioxide, the reference phonon frequencies and Grüneisen parameters were approximated using the values obtained at the MP2/CBS limit. See Ref 28 for details.

During the structure optimization and lattice dynamics calculations, the HMBI MM contributions were computed with the Amoeba polarizable force field[64,65] and Tinker 6.3.[66] Force field parameters for carbon dioxide were computed using Poltype[67] as described in Ref 28. A subsequent set of single-point energy refinements reported here replace the MM contribution with one evaluated using our *ab initio* force field (AIFF).[34,68,69] The AIFF includes multipolar two-body electrostatics (up to hexadecapole), many-body polarization, two- and three-body dispersion. These contributions are represented in terms of distributed multipoles, distributed polarizabilities, and distributed dispersion coefficients which are computed using asymptotically corrected PBE0 density functional theory and aug-cc-pVTZ basis with CamCasp 5.6.[70]

For each crystal, the following steps were repeated with each electronic structure method/basis set combination:

1. The crystal structure was first optimized with respect to the HMBI electronic energy using a given method/basis set and Amoeba MM terms. Phonons were computed at the same level of theory using lattice dynamics with a 3×3×3 supercell and a 3×3×3 Monkhorst-Pack k-point grid. In test calculations on carbon dioxide, using a larger 5×5×5 supercell alters the vibrational free energies by less than 0.05 kJ/mol (see supporting information). These calculations provide the initial structure, reference unit cell volume V^{ref}, and reference frequencies $\omega_{k,i}^{ref}$ used in the quasi-harmonic approximation. Gas-phase molecules were optimized using the same electronic structure method and basis set as the crystal.

2. Mode-specific Grüneisen parameters (Eq 4) were obtained via finite difference between phonon frequencies obtained at two distinct unit cell volumes. Specifically, the optimized unit cells from Step 1 were separately expanded and contracted isotropically by

10 Å^3. For each of these new unit cell dimensions, the atomic coordinates were relaxed subject to fixed lattice parameters. Lattice dynamics phonon calculations were performed on each optimized structure. Overlap of the normal mode eigenvectors was used to ensure proper assignment of the frequencies between the two structures in the finite difference. Test calculations indicate that changing the finite-difference step size to 8 Å^3 or 12 Å^3 alters the resulting vibrational free energies in carbon dioxide or acetic acid by less than ∼0.1 kJ/mol over the relevant volume ranges (see supporting information).

3. Quasi-harmonic Gibbs free energy optimizations were then performed for each species at each of several different temperatures. These calculations allow the unit cell to relax due to zero-point energy and thermal expansion. The vibrational free energy contribution to the crystal was estimated as a function of temperature and unit cell volume according to Eqs 3 and 5. A pressure of 1 atm was used in all cases. The PV term is negligible in the solid at this pressure and was omitted, but it was included as an RT term in the gas-phase free energies (Eq 14).

4. For each temperature, the enthalpies, entropies, and Gibbs free energies of sublimation were computed at the same level of theory using the structures and quasi-harmonic frequencies obtained from Step 3.

5. A second set of enthalpies of sublimation was computed for each geometry from Step 3 in which the single-point electronic energy contributions (e.g. U_{el} in Eq 1) is computed using CCSD(T)/CBS QM and AIFF MM. Comparing these single-point enthalpies at the same, high level of theory using geometries obtained with different basis sets helps decouple the effects of crystal structure and electronic structure method/basis set on the predicted enthalpies of sublimation.

6. Finally, the volumes, enthalpies, entropies, and Gibbs free energies were also evaluated without the quasi-harmonic approximation (denoted "No QHA" in figures and tables).

In this case, the electronic energy optimized structures and the reference phonon frequencies from Step 1 are assumed not to change with temperature when evaluating the various statistical mechanics expressions in Section 2.2.

Both carbon dioxide and ice expand isotropically, so the use of isotropic scaling of the unit cell when computing the Grüneisen parameters is reasonable. The other two crystals exhibit more anisotropic expansion. A better algorithm might vary the unit cell volume through the application of external pressure, though that was not done here. Nevertheless, the results presented below still achieve good agreement with the experimental thermochemical data.

Computationally, there are two main bottlenecks in these calculations. The first is the calculation of the reference phonons and Grüneisen parameters. Though the fragment approach means that only monomer and dimer Hessian calculations are needed at the QM level, these are still moderately expensive at the large-basis MP2 level. In the approach described above, three sets of Hessian calculations are needed for a given crystal: one for the reference phonon frequencies and two more for the finite difference over phonon frequencies to compute the mode-specific Grüneisen parameters. For MP2, analytic Hessians were not available, so each monomer or dimer fragment Hessian calculation is performed via finite difference of the nuclear gradients. Even exploiting space group symmetry,[52] an MP2/atz Hessian calculation on crystalline imidazole requires nearly 7,500 dimer force calculations (due to the many possible finite displacements of the nuclei), or about ∼6,500 Intel Xeon E5-2680v3 CPU hours on a standard compute node of the Comet supercomputer at the San Diego Supercomputer Center. This amounts to roughly ∼20,000 hours to perform all three sets of Hessian calculations. Of course, each of those 7,500 dimer calculations can be performed in parallel on a separate processor or processor group, so the wall time requirements are much lower.

Second, use of the quasi-harmonic approximation means that the geometry must be optimized for each new temperature (or pressure). After exploiting space group symmetry, each optimization cycle for crystalline imidazole required ∼65–70 dimer calculations, or about

55-60 CPU hours for MP2/aTZ on Comet. Again, each dimer job can be run simultaneously on separate processors to achieve shorter wall times. With the DL-FIND geometry optimizer[71] used in our code, a complete geometry optimization typically requires ∼10-50 geometry optimization cycles, or ∼500-3,000 CPU hours per temperature.

In other words, obtaining reference phonon frequencies and Grüneisen parameters incurs steep computational costs at the outset. However, those quantities can be re-used for each temperature (or pressure) considered. Therefore, if one is interested in scanning a large region of the phase diagram, the cost of performing repeated geometry optimizations can readily exceed the cost associated with obtaining the phonons. Nevertheless, it may be worthwhile investigating further approximations for the phonons/Grüneisen parameters (e.g. perhaps computing them from a less expensive model like DFT).

The specific electronic structure methods and basis sets applied to each of the four crystals depends on the computational cost. For carbon dioxide, the small size of the molecule and high symmetry in the phase I crystal enabled geometry optimizations using up to MP2/CBS and even the estimated CCSD(T)/CBS limit. Despite the absence of useful symmetry in ice Ih, the small size of water molecules enabled optimizations up to the MP2/CBS limit. Post-MP2 corrections to the ice lattice energy and lattice constants are small,[30,72] so coupled cluster calculations were not performed on that crystal. Due to their larger molecular sizes, the acetic acid and imidazole crystal optimizations were performed using only the smaller aDZ and aTZ basis sets.

4 Results and Discussion

The following sections examine the convergence of the predicted molar volume, enthalpy of sublimation, and entropy of sublimation for each of the four crystals both with respect to the method/basis set and relative to experiment. Experimental molar volumes were obtained directly from the literature. The enthalpies and entropies of sublimation were mostly derived

empirically using experimental data found in the literature, as described in the Appendix.

Experimental uncertainties were not reported for many of the individual contributions used to derive the enthalpies and entropies of sublimation. For enthalpies of sublimation, it is not unusual to find values reported in the literature that differ by several kJ/mol. For instance, the ΔH_{sub} values reported for imidazole by Chickos and Acree[73] in the vicinity of room temperature vary from ∼75–85 kJ/mol. Even if one discards the largest outlier (74.5 kJ/mol), the remaining values span a 5 kJ/mol range. Appreciable errors are also likely for the empirical entropies of sublimation.

Finally, note that the some of the carbon dioxide data reported here comes from an earlier publication, while other data is new. Specifically, the volumes in Figure 2, sublimation enthalpies in Figure 3a, and sublimation entropies in Figure 4a have been reported previously,[28] while the CCSD(T)/CBS + AIFF enthalpies in Figure 3b and sublimation temperatures in Table 3 are new here. The data for the other three crystals is reported here for the first time.

4.1 Molar Volumes

The predicted molar volumes of each crystal were computed as a function of temperature using several different electronic structure method/basis set combinations. These results are compared against the corresponding experimental data in Figure 2. The "No QHA" data in Figure 2 refers to the structures obtained by minimizing the electronic energy instead of the quasi-harmonic Gibbs free energy.

Experimental temperature-dependent volume data for carbon dioxide and ice were obtained from Refs 74 and 75, respectively. Experimental volumes for acetic acid at 40 K (RefCode ACETAC07),[76] 83 K (ACETAC02),[49] 133 K (ACETAC03),[77] and 278 K (ACETAC01)[49] were found in the Cambridge Structure Database. Experimental volumes for imidazole were similarly obtained at 103 K (IMAZOL06),[50] 123 K (IMAZOL04),[78] 173 K (IMAZOL14),[79] and room temperature.[78,80,81] The Cambridge database contains three differ-

Table 1: Percent molar volume expansion arising from the zero-point vibrational energy and thermal vibrational contributions. Percentages are reported relative to the electronic energy minimized structure (no QHA).

Crystal	Structures	T_{max}	Zero-Point[a]	Thermal[b]	Total
Carbon Dioxide	CCSD(T)/CBS	190 K	2.9%	7.6%	10.5%
Ice	MP2/CBS	265 K	3.3%	2.1%	5.4%
Acetic acid	MP2/aTZ	278 K	2.1%	5.6%	7.7%
Imidazole	MP2/aTZ	283 K	2.1%	4.2%	6.3%

[a] Expansion between the structures optimized at 0 K with and without quasi-harmonic zero-point vibrational energy.

[b] Quasi-harmonic thermal expansion occurring between 0 K and T_{max}.

ent room-temperature structures for imidazole: 55.18 cm^3/mol (IMAZOL05), 54.41 cm^3/mol (IMAZOL10), and 55.23 cm^3/mol (IMAZOL13). All three values are reported here.

Before studying the performance of various models in detail, we examine broad trends associated with the thermal expansion. Table 1 summarizes the predicted percent expansions using the highest-level model chemistry reported for each crystal. First, we observe that ice expands the least (5.4%), while carbon dioxide expands the most (10.5%). The 6–8% percent expansion for the other two crystals lies in between these two extremes. These expansion trends can be rationalized based on the crystal packing. Carbon dioxide is held together primarily by relatively weak quadrupolar and van der Waals interactions, which allow for substantial expansion. In contrast, the strong three-dimensional hydrogen bond network in ice inhibits thermal expansion. The other two crystals exhibit one-dimensional hydrogen-bonded chains. Thermal expansion is hindered along the hydrogen bond chain directions, but it occurs more readily in directions orthogonal to the chains.

Second, Table 1 decomposes the total expansion into the portion which occurs solely due to zero-point vibrational energy (ZPVE) and the portion which arises from the finite-temperature contributions. The former is the difference between the volumes of the electronic energy minimized structures ("No QHA") and the 0 K structures. The latter reports the expansion between the 0 K and maximum temperature structures considered. The expansion behaviors of the four crystals are also evident in Figure 2. In all cases, zero-point vibrational

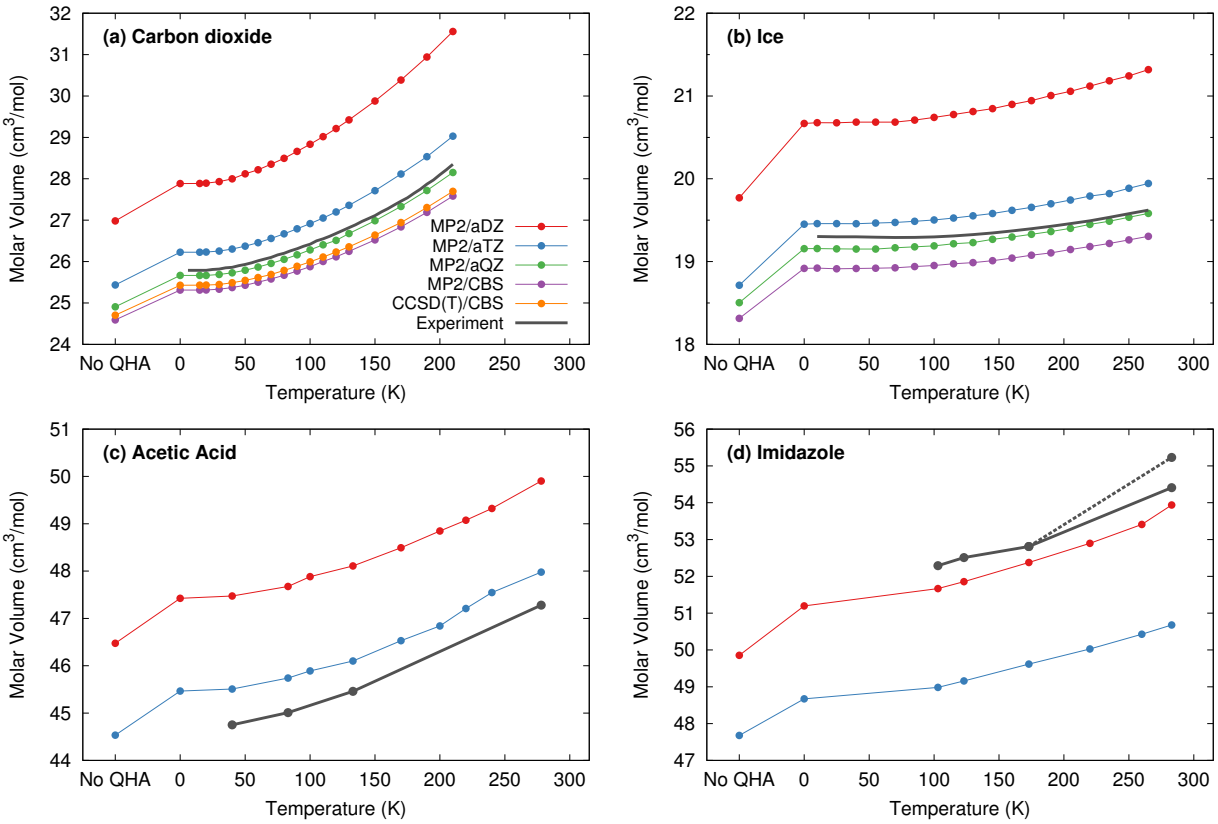

Figure 2: Predicted thermal expansion of crystalline carbon dioxide, ice, acetic acid, and imidazole. The "No QHA" volumes were obtained via conventional minimization of the electronic energy.

energy drives a substantial fraction of the overall expansion. In ice, 60% of the overall expansion occurs due to zero-point energy. Zero-point expansion represents a smaller fraction of the overall expansion in the other three crystals, but it still amounts to almost a third of the total expansion.

Next, we focus on the detailed performance of the models for individual crystals. We previously[28] examined the thermal expansion of phase I carbon dioxide using basis sets of increasing size up to the MP2/CBS and CCSD(T)/CBS levels. These results are repeated in Figure 2a for comparison with the other three crystals. The predicted MP2/aDZ molar volume is significantly too large at low temperatures, and its rate of expansion with increasing temperature is overestimated compared to experiment. Increasing the basis set toward the CBS limit decreases the volume for all temperatures, improving the agreement with ex-

periment. In the CBS limit, MP2 underestimates the low-temperature volume, and this is slightly corrected at the CCSD(T) level. This underestimation probably occurs in part due to the neglect of repulsive three-body dispersion, which is significant in carbon dioxide.[82] Using the larger basis sets also improves the rate of thermal expansion with temperature, producing expansion curves that are nearly parallel to the experimental one.

Similar behavior is observed for ice. MP2/aDZ substantially overestimates the molar volume at all temperatures, but using larger basis sets produces volumes that agree with experiment to within 0.4 cm^3/mol or less. Once again, MP2/aQZ and MP2/CBS underestimate the molar volume. The models also modestly overestimate the amount of thermal expansion in ice, most notably at higher temperatures. Experimentally, the crystal expands by 1.6% between 10 K and 265 K. Over the same range, the quasi-harmonic MP2 calculations predict expansion of 3.1%, 2.5%, 2.2%, and 2.0% as the basis is increased along the series aDZ, aTZ, aQZ, and extrapolated to the CBS limit, respectively. Increasing the basis set size improves the predicted amountof thermal expansion relative to experiment, just as was seen for carbon dioxide.

Ice Ih is unusual in that it exhibits negative thermal expansion (i.e. the volume actually decreases with increasing temperature) at low temperatures. Experimentally, the volume at 70 K (roughly the minimum) is 0.06% smaller than the volume at 10 K. The MP2/aDZ predictions miss this negative thermal expansion entirely. The larger-basis set calculations do capture the correct qualitative behavior, though they are not quantitatively correct. The predicted volume decreases range from less than -0.01% in MP2/aTZ to -0.04% for MP2/CBS). The models also underestimate the temperature range over which the negative expansion occurs. Both MP2/aTZ and MP2/aQZ predict a minimum volume around 40 K and MP2/CBS predicts the minimum around 25 K, compared to 70 K experimentally.

Previous studies indicate that the electronic energy minimum structure and the lattice energy change little between MP2 and CCSD(T) treatments of the one-body and two-body terms,[30,72] so it seems unlikely that performing coupled cluster calculations would alter the

MP2 predictions significantly. The residual errors here most likely stem from the force field treatment of the strong many-body polarization effects which arise from cooperative hydrogen bonding and/or from the quasi-harmonic treatment. It would be instructive to examine to what extent a more elaborate many-body water potential[83,84] could correct the residual errors.

Like carbon dioxide and ice, the acetic acid molar volume improves as the basis set is increased from aDZ to aTZ. MP2/aDZ and MP2/aTZ consistently overestimate the volume by $\sim$2.5 cm^3/mol and $\sim$0.7 cm^3/mol, respectively. The acetic acid quasi-harmonic optimizations suffered from minor numerical convergence issues (particularly for MP2/aDZ) which led to the slight roughness in the predicted expansion curves, but both curves are generally parallel to the experimental one. Experimentally, the acetic acid crystal expands by 5.6% between 40 K and 278 K, versus expansion of 5.3% and 5.4% with MP2/aDZ and aTZ respectively. Based on the trends observed for carbon dioxide and ice, one might anticipate smaller errors and improved parallelarity in a larger aQZ basis set. Those calculations were not performed, however, due to their high computational expense.

Finally, imidazole provides an interesting case. In the previous three crystals, MP2/aDZ substantially overestimated the crystal volume, and larger basis sets correct this. In imidazole, MP2/aDZ already slightly underestimates the volume but is (fortuitously) in excellent agreement with the experimental volumes. Increasing the basis set from aDZ to aTZ shrinks the volume further, leading to much larger errors.

The problem stems from the strong π-electron van der Waals interactions in imidazole. MP2 exhibits known problems overestimating the strength of such non-covalent interactions.[85,86] Similarly, MP2 overestimates the lattice energy of crystalline imidazole by 10–15% compared to CCSD(T).[30,34] This overbinding apparently leads to a crystal structure that is too dense. From a practical point of view, this is potentially problematic for optimizing such structures with fragment-based methods. Coupled cluster theory corrects these weaknesses of MP2, but such calculations are generally too expensive for crystal structure optimization

beyond the simplest crystals. Applying a dispersion correction to MP2 as in the MP2C model[87,88] helps, but analytic gradients of MP2C are not currently available. At present, dispersion-corrected periodic density functional theory methods probably provide the best alternative for optimizing such crystals.[89–91]

As noted earlier, several experimental values have been reported for the molar volume of imidazole at 283 K: two values around 55.2 cm^3/mol, and one at 54.4 cm^3/mol (a difference of about 1.5%). The predicted thermal expansion of MP2/aDZ exhibits an increased slope above 260 K that could support the two larger experimental volumes, while the flatter slope of the MP2/aTZ thermal expansion curve is in better qualitative agreement with the smaller experimental volume. Unfortunately, the predictions here do not appear reliable enough to adjudicate among the different reported experimental volumes.

Overall, the thermal expansion results discussed here have a few important general implications. First, the quasi-harmonic approximation reproduces the thermal expansion fairly well in small, mostly rigid molecule crystals like these. Basis sets of at least triple-zeta quality appear to be necessary to achieve fairly good volume agreement with experiment, though the larger basis sets do slightly underestimate the volumes in carbon dioxide and ice.

Second, unit cell volumes predicted by minimizing the electronic energy clearly differ substantially from those observed experimentally at room temperatures. Based on the crystals examined here and other studies,[92,93] the volume expansion lies in the range of ∼5–10%, especially if one also considers the zero-point expansion.

Third, it is common to benchmark models by comparing predictions against low-temperature crystal structures.[94] The results here highlight crystal structure optimizations which neglect zero-point vibrational energy should actually be a few percent smaller in volume than the low-temperature experimental structures. In practice, small double-zeta basis sets have often been used in fragment-based model crystal structure optimizations. Assuming the pairwise interactions are counterpoise-corrected for basis set superposition error as in the calculations here, double-zeta basis sets consistently underbind the molecules (see Section 4.2) and over-

estimate the unit cell volume. This fortuitously leads to partial error cancellation between the small basis set and the neglect of zero-point contributions.

4.2 Enthalpy of Sublimation

The previous section demonstrates that one can predict temperature-dependent volumes for simple crystals consisting of small, rigid molecules fairly well using a quasi-harmonic approximation. The next question is how important is treating thermal expansion for predicting other crystal properties at finite temperatures? Given the general interest in predicting polymorph/phase stability, we focus on the enthalpies (this section), entropies, and Gibbs free energies (following sections) of sublimation here.

Figure 3 plots the predicted temperature-dependent sublimation enthalpies for each of the four crystals against the experimental values. The left column (Figures 3a–d) reports the enthalpies obtained by optimizing the crystal structure and evaluating the electronic energy with a given level of theory (e.g. MP2/aTZ), and it compares the results with (solid lines) and without (dotted lines) the quasi-harmonic approximation. The right column (Figures 3e–h) plots the same enthalpies, except with the electronic energy U_{el} at each data point replaced with a single-point energy on that structure evaluated using extrapolated CCSD(T)/CBS QM and AIFF force field MM contributions (instead of Amoeba MM).

Consider first Figures 3a–d. As discussed previously,[28] large-basis sets and the quasi-harmonic approximation are important for capturing the correct temperature-dependence of the sublimation enthalpy in carbon dioxide. In the absence of the quasi-harmonic approximation, the enthalpy is overestimated at high temperatures. Fortuitously, quasi-harmonic MP2/aQZ reproduces the experimental carbon dioxide enthalpies almost perfectly, while MP2/CBS and CCSD(T)/CBS slightly overestimate them by $\sim$1 kJ/mol.

The use of large basis sets is similarly important for the sublimation enthalpies in the other crystals. The largest jump occurs between the aDZ and aTZ basis sets, though the effects of larger basis sets still account for several kJ/mol. This matches earlier observations

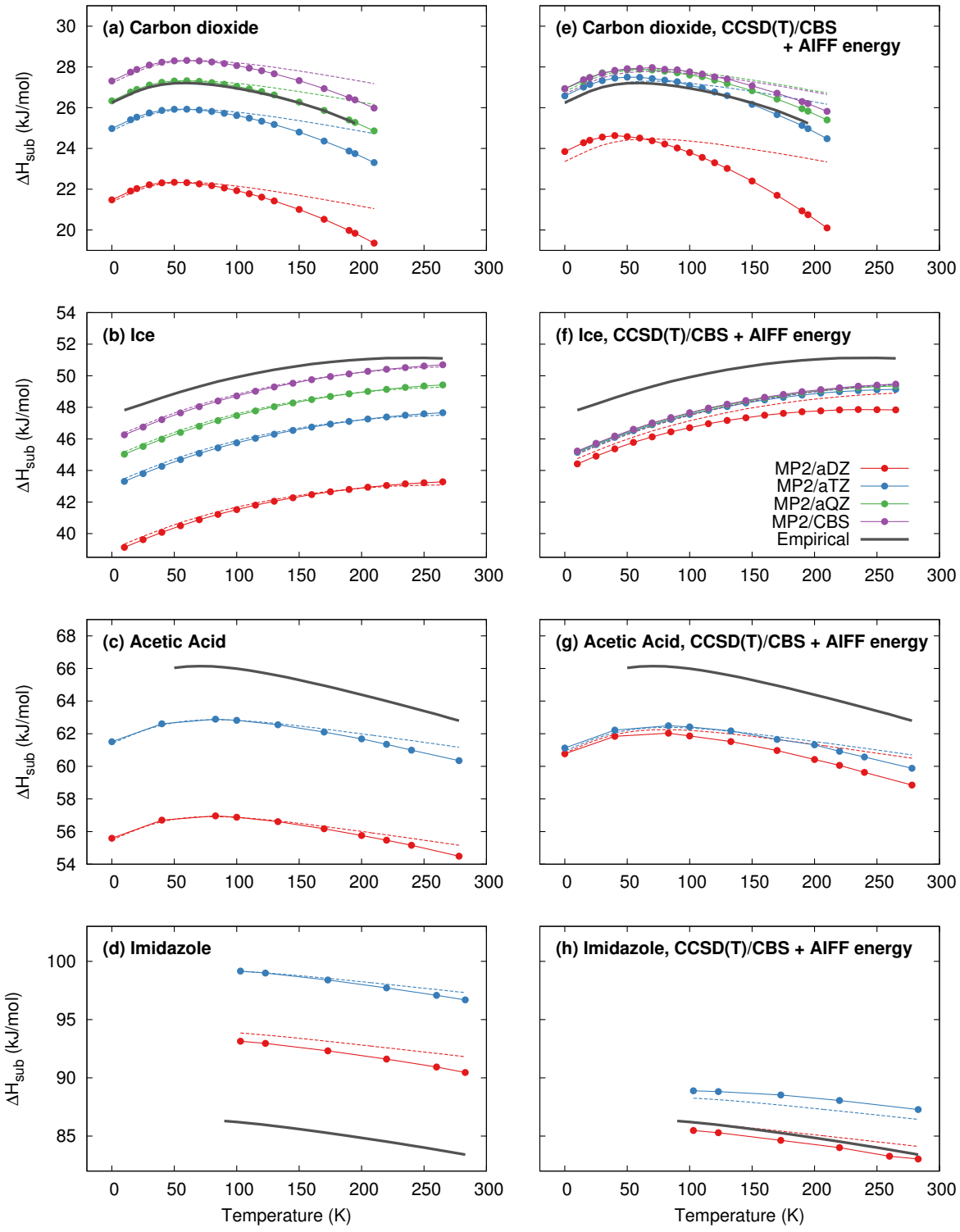

Figure 3: Predicted enthalpies of sublimation at 1 atm. Figures on the left use the same level of theory (e.g. MP2/aXZ + Amoeba) to optimize the structure and compute the sublimation enthalpy. Those on the right replace the lattice energy with single-point energies computed using CCSD(T)/CBS + AIFF. Curves drawn with solid lines include quasi-harmonic thermal expansion, while dotted lines neglect it.

for lattice energies. Like carbon dioxide, increasing basis set size improves the agreement of the sublimation enthalpy with experiment for ice and acetic acid. In imidazole, however, MP2 substantially overestimates the lattice energy,[30,34] which translates to a significant overestimation of the sublimation enthalpy. Agreement with the experimental enthalpy actually deteriorates with increasing basis set size in imidazole.

Though significant basis-set dependence is observed in Figures 3a–d, it is unclear to what extent this behavior reflects changes in the optimized crystal structure versus differences in the lattice energy. To decouple these two effects, Figures 3e–h re-compute the lattice energies U_{el} for every geometries using CCSD(T)/CBS plus AIFF MM terms. Doing so dramatically reduces the differences in sublimation enthalpy across the structures optimized with various basis sets. For ice and carbon dioxide, the structures computed with MP2/aTZ or better produce CCSD(T)/CBS sublimation enthalpies that are nearly indistinguishable. For all four crystals, enthalpies computed on the MP2/aDZ structures are only moderately worse, though MP2/aDZ does not capture the temperature dependence as well at higher temperatures.

For all temperatures, the CCSD(T) accuracy on the larger-basis structures here lies within ∼1 kJ/mol of the experimental sublimation enthalpies for carbon dioxide and within ∼3–4 kJ/mol for the other three crystals. Most notably, using CCSD(T) instead of MP2 for U_{el} also corrects a substantial portion of the error in the imidazole sublimation enthalpies, as one might expect from earlier studies of the lattice energy.[30,34] As discussed earlier, errors in the experimentally-derived sublimation enthalpies themselves are also probably up to several kJ/mol.

It is interesting to consider the difference between the lattice energy as computed without consideration of temperature and the finite-temperature sublimation enthalpy. Table 2 compares the CCSD(T)/CBS + AIFF lattice energy at the electronic energy minimum structure (using the largest-basis structure optimization) to the sublimation enthalpy at the maximum temperature computed here. In all four crystals, the lattice energy is 4–10 kJ/mol larger than the sublimation enthalpy, which amount to up to 20% error. Zero-point vibrational and

Table 2: Comparison between the electronic lattice energy and the quasi-harmonic sublimation enthalpy based on CCSD(T)/CBS + AIFF energies, in kJ/mol.

Crystal	Structure	$E_{lattice}$[a]	$\Delta H_{sub}(T)$[b]	Difference
Carbon Dioxide	CCSD(T)/CBS	29.7	26.3 (190 K)	4.1 (16%)
Ice	MP2/CBS	58.9	49.5 (265 K)	9.5 (19%)
Acetic acid	MP2/aTZ	66.0	59.9 (278 K)	6.2 (10%)
Imidazole	MP2/aTZ	91.6	87.3 (283 K)	4.3 (5%)

[a] Purely electronic lattice energy at the electronic energy minimum structure.
[b] Quasi-harmonic sublimation enthalpy at the highest temperature considered for each crystal.

finite-temperature effects clearly have a substantial impact on the thermodynamic stability of the crystal.

Finally, how important is thermal expansion? The answer depends on the degree of thermal expansion that occurs in the crystal. From Table 1, the amount of thermal expansion increases according to:

$$\text{ice} < \text{imidazole} < \text{acetic acid} < \text{CO}_2$$

As seen in Figure 3, the importance of quasi-harmonic thermal expansion behaves similarly. The differences between the enthalpies of ice predicted with and without thermal expansion are barely observable. Including thermal expansion when modeling imidazole leads to only a slight improvement in the slope of the enthalpy curve. For acetic acid and carbon dioxide, however, including thermal expansion clearly improves agreement with the experimental sublimation enthalpies. Without thermal expansion, the sublimation enthalpy in those species is overestimated at high temperatures. On the other hand, it is clear that the quantitative effects of thermal expansion on the enthalpies here are relatively small at ∼1–2 kJ/mol.

To summarize, temperature-dependent enthalpies of sublimation for these four crystals can be predicted to within a few kJ/mol. Large-basis sets (and sometimes post-MP2 correlation) are important for the lattice energy component. On the other hand, a triple-zeta basis is probably sufficient for the geometry optimization. The effects of thermal expansion on the sublimation enthalpies are modest—comparable to or smaller than the underlying errors

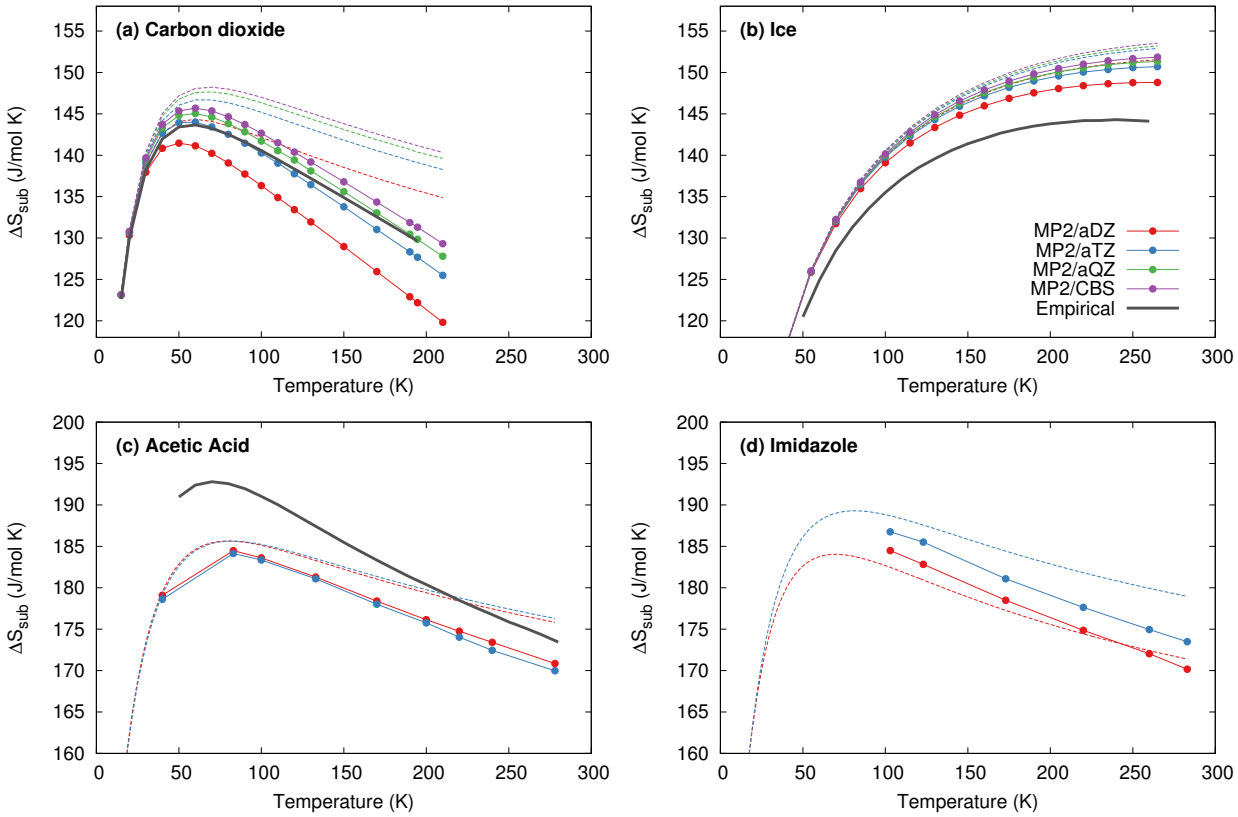

Figure 4: Predicted entropy of sublimation at 1 atm. Curves drawn with solid lines include quasi-harmonic thermal expansion, while dotted lines neglect it. Insufficient experimental data was available to derive an empirical sublimation entropy for imidazole.

in the predicted sublimation enthalpies. Unsurprisingly, thermal expansion becomes more important at high temperatures, especially in crystals that exhibit high thermal expansivity.

4.3 Entropy of Sublimation

Next we examine the predicted entropies of sublimation, which are plotted in Figure 4. As before, the solid lines correspond to the entropies predicted when including quasi-harmonic thermal expansion, while the dotted lines neglect thermal expansion. Note that we were unable to locate sufficient data to derive sublimation entropies for imidazole. The carbon dioxide entropies are identical to those reported previously.[28]

Two main features are notable in Figure 4. First, the sublimation entropies of carbon dioxide and imidazole both exhibit modest basis-set dependence, while the basis-set de-

pendence is much smaller for ice and acetic acid. In the latter two cases, the individual frequencies do exhibit the normal, expected variations with basis set, but these variations largely disappear in the summed vibrational entropy contributions.

Second, including thermal expansion clearly improves the agreement of the predicted sublimation entropies with the empirical values derived from experiment. Most notably, thermal expansion improves the slopes of the entropies at higher temperatures. Unsurprisingly, the impact of thermal expansion on the sublimation entropies is largest in the crystals which expand the most—carbon dioxide, acetic acid and imidazole. In carbon dioxide near the sublimation point (195 K), the MP2/CBS sublimation entropy is overestimated by 7% when thermal expansion is neglected. In acetic acid at 278 K, neglecting thermal expansion increases the sublimation entropy by 4% at the MP2/aTZ level. In imidazole, the MP2/aTZ error is 3% at 283 K. Viewed another way, neglecting thermal expansion in these cases introduces an error of about 1.5–2 kJ/mol in $T\Delta S$ near room temperature (or near the sublimation point in the case of carbon dioxide). That corresponds to about half the magnitude of the error in the CCSD(T)/CBS sublimation enthalpies. For ice, in contrast, the small degree of thermal expansion alters the MP2/CBS sublimation entropy by only 1% at 265 K, or $\sim$0.5 kJ/mol in $T\Delta S$.

4.4 Gibbs Free Energy of Sublimation

Finally, one might combine the enthalpies and entropies of sublimation to predict the Gibbs free energy and determine phase stability. Given the sparsity of temperatures with enthalpy and entropy data for each crystal (especially experimentally), Gibbs free energy curves were generated as a function of temperature by smoothing and splining over the available data. Based on these curves, Figure 5 plots the errors between the predicted and empirical sublimation enthalpies, entropies (as $-T\Delta S$), and free energies. The enthalpies here are the CCSD(T)/CBS + AIFF results using the MP2/CBS geometries (or MP2/aTZ for acetic acid). The entropies used were computed at the same level as the geometry optimizations.

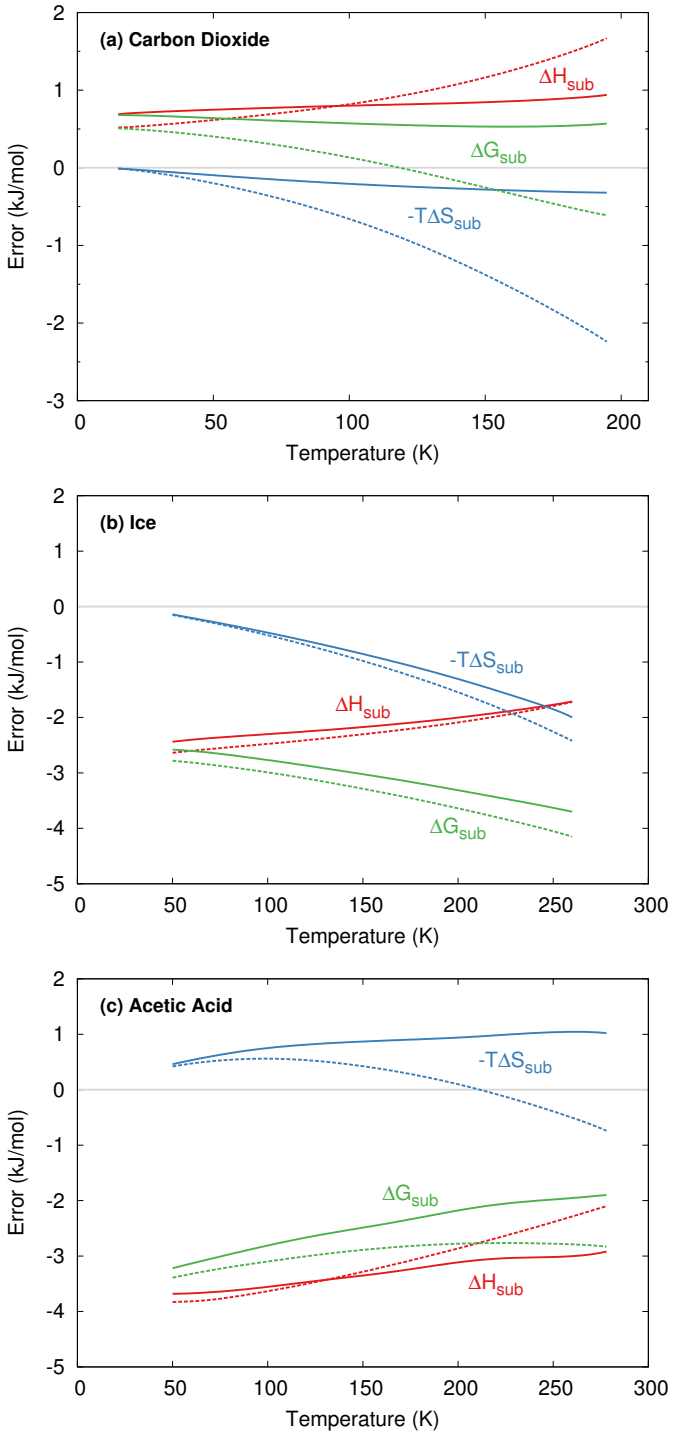

Figure 5: Estimated errors in the predicted enthalpies, entropies, and Gibbs free energies of sublimation relative to experiment. Curves were generated by smoothing and splining the available experimental and predicted values. Predictions with (solid lines) and without (dotted lines) quasi-harmonic expansion are shown.

Imidazole is excluded from this analysis due to the lack of experimental entropy data.

For the three crystals shown here, the sublimation free energy errors range from ∼0.5 kJ/mol in carbon dioxide to up to ∼4 kJ/mol in ice. For carbon and dioxide, the errors in ΔH and $-T\Delta S$ have opposite signs and cancel somewhat when combined into the free energy. For ice, on the other hand, the errors have the same sign, and the error in the free energy is larger.

Focus now on the error introduced by neglecting thermal expansion. Figure 5 makes it clear that thermal expansion is more important for the entropy than the enthalpy at high temperatures. However, the errors due to ignoring thermal expansion in carbon dioxide and acetic acid partially cancel between the enthalpy and entropy at higher temperatures. The resulting differences in the free energies with and without thermal expansion are ∼1 kJ/mol at the highest temperatures modeled. For ice, the thermal expansion errors in ΔH and $-T\Delta S$ do not cancel in ΔG for the temperature range considered here, but they remain small (< 0.5 kJ/mol).

To understand the cancellation of errors associated with thermal expansion, consider the temperature dependence of the enthalpy and entropy of sublimation and how crystal expansion affects them. Typically, the sublimation enthalpy initially rises with temperature before reaching a maximum and turning over. This behavior is readily apparent for carbon dioxide, acetic acid, and imidazole in Figure 3. For ice, this turnover is subtle and difficult to see in the plots—the experimental enthalpy decreases by less than 0.1 kJ/mol between its maximum around 240 K and 270 K.

In terms of internal energy, the crystal is more stable than the gas due to its favorable intermolecular interactions. Thermal contributions act to destabilize both phases. The temperature dependence of the gas-phase enthalpy is dominated by the translational and rotational contributions ($4RT$), while for the crystal it is dominated by destabilization of the lattice energy and the low-frequency mode vibrational contributions. Thermal expansion weakens the intermolecular interactions (hence the change in lattice energy). It can also

soften the intermolecular lattice phonon modes (though the phonon density of states is not strictly correlated with packing density[13]), which slightly stabilizes the crystal due primarily to reduction in zero-point energy. In the crystals exhibiting appreciable thermal expansion here, the changes in enthalpy are dominated by the decrease in lattice energy rather than the vibrational contributions.

At low temperatures, heating destabilizes the gas by a greater amount than for the crystal. At higher temperatures, the thermal destabilization of the crystal becomes more pronounced relative to the gas, creating the observed maximum in the sublimation enthalpy. If thermal expansion is neglected, however, the lattice energy does not decrease as it should. Accordingly, neglecting thermal expansion causes ΔH_{sub} to be overestimated at higher temperatures.

The entropy of the gas is much higher than that of the crystal, leading to a large, positive ΔS_{sub}. The sublimation entropy also exhibits a temperature dependence similar to that of the enthalpy, with a maximum at intermediate temperatures. Once again, the entropy of the gas increases by a greater amount at low temperatures, but at higher temperatures the low-frequency modes of the crystal dominate and cause the crystal entropy to rise by a greater amount than that of the gas. This transition produces the turnover observed in the sublimation entropies (Figure 4). Without thermal expansion, the lattice phonon frequencies are typically too large, and the entropic contribution to the crystal too small. Thus, ΔS_{sub} is overestimated at higher temperatures. Viewed another way, the entropy of the solid can be computed by integrating the ratio of the isobaric heat capacity to temperature C_p/T over temperature. The overestimation of the sublimation entropy when thermal expansion is neglected indicates that the isobaric heat capacity of the crystal is too small at higher temperatures. We previously showed that the (related) isochoric heat capacity C_v of carbon dioxide is indeed smaller when thermal expansion is neglected.[28] Note too that whereas thermal expansion generally destabilizes the enthalpy of the solid (unfavorable), it increases the entropy (favorable). In other words, thermal expansion is driven by entropy rather than

enthalpy.

In the end, neglecting thermal expansion typically leads to overestimation of both ΔH_{sub} (because the solid is bound too strongly) and ΔS_{sub} (because the entropy of the solid is underestimated). These enthalpy and entropy contributions enter the Gibbs free energy with opposite signs, meaning that the errors arising from the neglect of thermal expansion cancel somewhat. The ∼0.5–1 kJ/mol free energy errors associated with neglecting thermal expansion are smaller than the size of the overall errors in the sublimation free energies. On the other hand, about half the polymorph pairs in the Nyman and Day survey were separated by less than 2 kJ/mol (and many of those by <1 kJ/mol).[13] In other words, despite the small magnitude of these errors, thermal expansion might prove important for polymorphs with very similar free energies.

Finally, we use the computed Gibbs free energies to predict the sublimation point of carbon dioxide at 1 atm. We previously demonstrated[28] (1) a strong basis set dependence in the sublimation temperature, ranging from 163.6 K with MP2/aDZ to 199.2 K for MP2/CBS, and (2) that CCSD(T)/CBS + Amoeba calculations with thermal expansion slightly overestimate the sublimation point at 201.0 K, versus 194.7 K experimentally. Despite overestimating both the enthalpy and entropy of sublimation, the CCSD(T)/CBS model without thermal expansion predicts a sublimation point of 194.9 K due to fortuitous error cancellation.

Here, Table 3 revises these predictions by performing CCSD(T)/CBS + AIFF single-point energies on structures optimized with each level of theory. This both applies a uniformly high-level electronic structure model to the QM electronic energy terms in all cases, and it replaces the force field with the more accurate AIFF model that includes estimates for Axilrod-Teller-Muto three-body dispersion. As expected from Figure 3e, replacing the smaller-basis MP2 electronic energies with single-point CCSD(T)/CBS ones calculation substantially improves the sublimation enthalpies and eliminates much of the apparent basis set dependence in the predicted sublimation temperatures. The quasi-harmonic temperature predictions now vary

Table 3: Predicted sublimation temperatures for carbon dioxide using various electronic structure methods for the structure optimization/phonons and CCSD(T)/CBS + AIFF single point energies.

Structure	No Thermal Expansion			With Thermal Expansion		
	T_{sub} (K)	ΔH_{sub}(194.7 K) (kJ/mol)	ΔS_{sub}(194.7 K) (J/mol K)	T_{sub} (K)	ΔH_{sub}(194.7 K) (kJ/mol)	ΔS_{sub}(194.7 K) (J/mol K)
MP2/aDZ	192.0	26.1	135.7	190.6	23.3	122.2
MP2/aTZ	191.8	26.7	139.1	197.2	25.3	127.7
MP2/aQZ	192.0	27.0	140.3	198.3	25.9	129.8
MP2/CBS	190.3	26.9	141.2	198.7	26.3	131.3
CCSD(T)/CBS	190.4	26.9	141.1	198.0	26.2	131.3
Giauque and Egan[95]				194.7	25.2	129.6

from 190.6 K (MP2/aDZ structures) to 198.0 K (CCSD(T)/CBS structures)

The refined force field model also slightly decreases the sublimation enthalpies (due to the repulsive three-body dispersion), reducing the sublimation temperature by a few degrees Kelvin relative to the earlier work. Now both models with and without quasi-harmonic expansion lie within 3–4 K of the experimental sublimation temperature of 194.7 K. For comparison, a few degree change in the sublimation temperature corresponds to changing the sublimation enthalpy by ∼0.5 kJ/mol, which is smaller than the level of accuracy one can reasonably expect from the models. On the other hand, the quasi-harmonic model predicts the sublimation temperature reliably through accurate predictions of both the enthalpy and entropy, while the calculations without thermal expansion rely on large error cancellations between the overestimated enthalpies and entropies of sublimation.

5 Conclusions

In the end, the results here demonstrate that thermal expansion does indeed affect molecular crystal properties, though its significance will depend on the specific crystal and application. Unsurprisingly, the unit cell volume is most notably affected by thermal expansion. For the four crystals considered here, expansion of 5-10% is predicted between the electronic energy structures and structures near room temperature. A sizable fraction of the crystal expansion arises from zero-point vibrational energy. Accordingly, caution should be taken

when citing agreement between predicted electronic energy crystal structures which omit zero-point energy and low-temperature experimental structures which include it. Crystal properties that depend strongly on the distances and orientations of molecules, such as charge transport in organic semiconductor materials, will also likely be affected by these changes in unit cell volume with temperature.

For thermochemistry, neglecting thermal expansion leads to errors of up to a few kJ/mol. Errors in the free energy tend to be smaller than those in the enthalpy and entropy due to error cancellation, but they can still be of the same order of magnitude as the stability differences between many crystal polymorphs. Additional error cancellation might occur when comparing free energies between two different polymorphs, though the extent of that cancellation would likely depend on how similarly the crystals expand with temperature. In any case, for crystals in which the thermal expansion is appreciable and the energetic separations between polymorphs is small, neglecting thermal expansion might lead to an incorrect stability ordering.

Finally, the results here suggest that MP2/aug-cc-pVTZ provides a reasonable level of theory for optimizing crystal structures and calculating phonon modes, except in cases like imidazole where MP2 is known to have problems describing the van der Waals dispersion interactions. The smaller aug-cc-pVDZ basis set tends to overestimate the unit cell volume significantly. The improvements in geometries offered by quadruple-zeta basis sets or larger are small relative to the increase in computational costs. On the other hand, using larger basis sets is important for achieving quantitative accuracy in the lattice energy. Finally, the quasi-harmonic approach provides an effective tool for modeling thermal expansion and free energies, at least for small rigid molecules like the ones studied here. The performance of the quasi-harmonic model for conformationally flexible molecules requires future investigation.

A Appendix: Experimentally Derived Thermochemistry Data

The empirical enthalpies and entropies of sublimation used to validate the predictions were obtained as a function of temperature for each crystal as follows. Tabulations of the resulting empirical enthalpies and entropies of sublimation are provided as supporting information.

A.1 Carbon Dioxide

For carbon dioxide, temperature-dependent heats of sublimation at 1 atm were taken from Azreg-Aïnou.[96] The entropies of sublimation were derived according to:

$$\begin{aligned} \Delta S_{sub}^{empr}(T) &= \Delta S_{sub}^{expt}(194.7K) - \int_{194.7K}^{T} \frac{C_{p,solid}(T)}{T} dT \\ &\quad + (S_{gas}(T) - S_{gas}(194.7K)) \end{aligned} \tag{21}$$

This expression was evaluated using the sublimation entropy at 194.7 K[97] and heat capacities for the crystal[97] and gas-phase rotational constants[98] and vibrational frequencies.[99] See Ref 28 for details.

A.2 Ice Ih

Temperature-dependent experimental enthalpies of sublimation for ice Ih were taken from the equation of state of Feistel and Wagner.[100] Entropies of sublimation were derived from experimental data according to:

$$\begin{aligned} \Delta S_{sub}^{empr}(T) &= S_{gas}(T) - S_{gas}(373.15K) + \Delta S_{vap}(373.15K) \\ &\quad + S_{liquid}(373.15K) - S_{liquid}(273.15K) + \Delta S_{fus}(273.15K) \\ &\quad + \int_{T}^{273.15K} \frac{C_{p,solid}(T)}{T} dT \end{aligned} \tag{22}$$

The entropies for the gas and liquid water were found on the NIST/TRC Web Thermo Tables.[101] The entropy of vaporization and fusion were computed from the enthalpy of vaporization and fusion at their transition points ($\Delta S_{fus}(289.15K) = \frac{\Delta H_{fus}(289.15K)}{289.15K}$ and $\Delta S_{vap}(391.7K) = \frac{\Delta H_{vap}(391.7K)}{391.7K}$). The enthalpies of vaporization and fusion at their transition point were taken from the Handbook of Chemistry and Physics.[102] Isobaric heat capacities from Ref 103 were converted to a smooth function using a cubic spline and integrated using Mathematica.

Acetic Acid

For acetic acid, empirical enthalpies and entropies of sublimation were determined by combining a series of reported values:

$$\begin{aligned} \Delta H_{sub}^{empr}(T) &= H_{gas}(T) - H_{gas}(298.15K) + \Delta H_{vap}(298.15K) \\ &\quad + H_{liquid}(298.15K) - H_{liquid}(289.6K) + \Delta H_{fus}(289.6K) \\ &\quad + H_{solid}(289.6K) - H_{solid}(T) \end{aligned} \tag{23}$$

$$\begin{aligned} \Delta S_{sub}^{empr}(T) &= S_{gas}(T) - S_{gas}(391.7K) + \Delta S_{vap}(391.7K) \\ &\quad + S_{liquid}(391.7K) - S_{liquid}(289.6K) + \Delta S_{fus}(289.6K) \\ &\quad + S_{solid}(289.6K) - S_{solid}(T) \end{aligned} \tag{24}$$

The gas, liquid, and solid enthalpies ($H(T)$) and entropies ($S(T)$) at various temperatures were taken from the NIST/TRC Web Thermo Tables.[101] Values for the enthalpies of vaporization[104] and fusion[105] were taken from the literature. The entropies of vaporization and fusion were determined by dividing the corresponding enthalpy at the appropriate phase transition temperature ($\Delta S_{fus}(289.6K) = \frac{\Delta H_{fus}(289.6K)}{289.6K}$, $\Delta S_{vap}(391.7K) = \frac{\Delta H_{vap}(391.7K)}{391.7K}$). Since the enthalpy of vaporization was reported at 298.15 K instead of at the boiling point

of 391.7 K, it was extrapolated to 391.7 K using data from the NIST/TRC Web Thermo Thermo Tables:

$$\begin{aligned} \Delta H_{vap}(391.7K) &= \Delta H_{vap}(298.15K) + H_{gas}(391.7) - H_{gas}(298.15K) \\ &\quad -H_{liquid}(391.7) + H_{liquid}(298.15K) \end{aligned} \tag{25}$$

Imidazole

Empirical sublimation enthalpies for imidazole were derived similarly to the previous crystals:

$$\begin{aligned} \Delta H_{sub}^{empr}(T) &= \Delta H_{sub}(298.15K) + H_{gas}(T) - H_{gas}(298.15K) \\ &\quad + \int_{T}^{298.15K} C_{p,solid}(T)dT \end{aligned} \tag{26}$$

The enthalpy of sublimation at 298.15 K was reported by Jiménez et al.[106] Isobaric heat capacities for solid imidazole[107] were converted to a smooth function via cubic spline and integrated using Mathematica. The enthalpy of gaseous imidazole at various temperatures was computed using Eqs 14 and 15. Experimental vibrational frequencies were taken from Billes et al.[108] The gas-phase electronic energy contribution was omitted because the value temperature T cancels with the one at 298.15 K. Insufficient data was found to derive the empirical entropies of sublimation for imidazole.

Acknowledgments

Funding for this work from the National Science Foundation (CHE-1362465) and supercomputer time from XSEDE (TG-CHE110064) are gratefully acknowledged.

References

(1) Cruz-Cabeza, A. J.; Reutzel-Edens, S. M.; Bernstein, J. *Chem. Soc. Rev.* **2015**, *44*, 8619–8635.

(2) Chemburkar, S. R.; Bauer, J.; Deming, K.; Spiwek, H.; Patel, K.; Morris, J.; Henry, R.; Spanton, S.; Dziki, W.; Porter, W.; Quick, J.; Bauer, P.; Donaubauer, J.; Narayanan, B. A.; Soldani, M.; Riley, D.; Mcfarland, K. *Org. Proc. Res. Dev.* **2000**, *4*, 413–417.

(3) Bauer, J.; Spanton, S.; Quick, R.; Quick, J.; Dziki, W.; Porter, W.; Morris, J. *Pharm. Res.* **2001**, *18*, 859–866.

(4) Raw, A. S.; Furness, M. S.; Gill, D. S.; Adams, R. C.; Holcombe, F. O.; Yu, L. X. *Adv. Drug Deliv. Rev.* **2004**, *56*, 397–414.

(5) G. Goldbeck, E. Pidcock, and C. Groom, "Solid Form Informatics for pharmaceuticals and agrochemicals: Knowledge-based substance development and risk assessment." Cambridge Crystallographic Data Center, 2012. `https://www.ccdc.cam.ac.uk/support-and-resources/ccdcresources/Solid_Form_Informati` Accessed March 14, 2016.

(6) Lommerse, J. P. M.; Motherwell, W. D. S.; Ammon, H. L.; Dunitz, J. D.; Gavezzotti, A.; Hofmann, D. W. M.; Leusen, F. J. J.; Mooij, W. T. M.; Price, S. L.; Schweizer, B.; Schmidt, M. U.; van Eijck, B. P.; Verwer, P.; Williams, D. E. *Acta Cryst. B* **2000**, *56*, 697–714.

(7) Motherwell, W. D. S.; Ammon, H. L.; Dunitz, J. D.; Dzyabchenko, A.; Erk, P.; Gavezzotti, A.; Hofmann, D. W. M.; Leusen, F. J. J.; Lommerse, J. P. M.; Mooij, W. T. M.; Price, S. L.; Scheraga, H. A.; Schweizer, B.; Schmidt, M. U.; van Eijck, B. P.; Verwer, P.; Williams, D. E. *Acta Cryst. B* **2002**, *58*, 647–661.

(8) Day, G. M.; Motherwell, W. D. S.; Ammon, H. L.; Boerrigter, S. X. M.; Della Valle, R. G.; Venuti, E.; Dzyabchenko, A.; Dunitz, J. D.; Schweizer, B.; van Eijck, B. P.; Erk, P.; Facelli, J. C.; Bazterra, V. E.; Ferraro, M. B.; Hofmann, D. W. M.; Leusen, F. J. J.; Liang, C.; Pantelides, C. C.; Karamertzanis, P. G.; Price, S. L.; Lewis, T. C.; Nowell, H.; Torrisi, A.; Scheraga, H. A.; Arnautova, Y. A.; Schmidt, M. U.; Verwer, P. *Acta Cryst. B* **2005**, *61*, 511–27.

(9) Day, G. M.; Cooper, T. G.; Cruz-Cabeza, A. J.; Hejczyk, K. E.; Ammon, H. L.; Boerrigter, S. X. M.; Tan, J. S.; Della Valle, R. G.; Venuti, E.; Jose, J.; Gadre, S. R.; Desiraju, G. R.; Thakur, T. S.; van Eijck, B. P.; Facelli, J. C.; Bazterra, V. E.; Ferraro, M. B.; Hofmann, D. W. M.; Neumann, M. A.; Leusen, F. J. J.; Kendrick, J.; Price, S. L.; Misquitta, A. J.; Karamertzanis, P. G.; Welch, G. W. A.; Scheraga, H. A.; Arnautova, Y. A.; Schmidt, M. U.; van de Streek, J.; Wolf, A. K.; Schweizer, B. *Acta Cryst. B* **2009**, *65*, 107–25.

(10) Bardwell, D. A.; Adjiman, C. S.; Arnautova, Y. A.; Bartashevich, E.; Boerrigter, S. X. M.; Braun, D. E.; Cruz-Cabeza, A. J.; Day, G. M.; Della Valle, R. G.; Desiraju, G. R.; van Eijck, B. P.; Facelli, J. C.; Ferraro, M. B.; Grillo, D.; Habgood, M.; Hofmann, D. W. M.; Hofmann, F.; Jose, K. V. J.; Karamertzanis, P. G.; Kazantsev, A. V.; Kendrick, J.; Kuleshova, L. N.; Leusen, F. J. J.; Maleev, A. V.; Misquitta, A. J.; Mohamed, S.; Needs, R. J.; Neumann, M. A.; Nikylov, D.; Orendt, A. M.; Pal, R.; Pantelides, C. C.; Pickard, C. J.; Price, L. S.; Price, S. L.; Scheraga, H. A.; van de Streek, J.; Thakur, T. S.; Tiwari, S.; Venuti, E.; Zhitkov, I. K. *Acta Cryst. B* **2011**, *67*, 535–51.

(11) Price, S. L. *Chem. Soc. Rev.* **2014**, *43*, 2098–111.

(12) Gavezzotti, A.; Filippini, G. *J. Am. Chem. Soc.* **1995**, *117*, 12299–12305.

(13) Nyman, J.; Day, G. M. *CrystEngComm* **2015**, *17*, 5154–5165.

(14) van Eijck, B. P. *J. Comp. Chem.* **2001**, *22*, 816–826.

(15) Anghel, A. T.; Day, G. M.; Price, S. L. *CrystEngComm* **2002**, *4*, 348.

(16) Rivera, S. A.; Allis, D. G.; Hudson, B. S. *Cryst. Growth Des.* **2008**, *8*, 3905–3907.

(17) Cruz-Cabeza, A. J.; Day, G. M.; Jones, W. *Chem. Eur. J.* **2008**, *14*, 8830–8836.

(18) Reilly, A. M.; Tkatchenko, A. *Phys. Rev. Lett.* **2014**, *113*, 055701.

(19) Price, S. L. *Acta Cryst. B* **2013**, *69*, 313–28.

(20) Raiteri, P.; Martonák, R.; Parrinello, M. *Angew. Chem. Int. Ed.* **2005**, *44*, 3769–73.

(21) Karamertzanis, P. G.; Raiteri, P.; Parrinello, M.; Leslie, M.; Price, S. L. *J. Phys. Chem. B* **2008**, *112*, 4298–308.

(22) Zykova-Timan, T.; Raiteri, P.; Parrinello, M. *J. Phys. Chem. B* **2008**, *112*, 13231–7.

(23) Coropceanu, V.; Cornil, J.; da Silva Filho, D. A.; Olivier, Y.; Silbey, R.; Brédas, J.-L. *Chem. Rev.* **2007**, *107*, 926–952.

(24) Li, Y.; Coropceanu, V.; Bredas, J.-L. *J. Phys. Chem. Lett.* **2012**, *3*, 3325–3329.

(25) Allan, N. L.; Barrera, G. D.; Barron, T. H. K.; Taylor, M. B. *Int. J. Thermophys.* **2001**, *22*, 535–546.

(26) Baroni, S.; de Gironcoli, S.; Dal Corso, A.; Giannozzi, P. *Rev. Mod. Phys.* **2001**, *73*, 516–562.

(27) Otero-de-la Roza, A.; Abbasi-Pérez, D.; Luaña, V. *Comput. Phys. Comm.* **2011**, *182*, 2232–2248.

(28) Heit, Y. N.; Nanda, K. D.; Beran, G. J. O. *Chem. Sci.* **2016**, *7*, 246.

(29) Beran, G. J. O. *J. Chem. Phys.* **2009**, *130*, 164115.

(30) Beran, G. J. O.; Nanda, K. *J. Phys. Chem. Lett.* **2010**, *1*, 3480–3487.

(31) Beran, G. J. O.; Wen, S.; Nanda, K.; Huang, Y.; Heit, Y. *Top. Curr. Chem.* **2014**, *345*, 59–93.

(32) Beran, G. J. O. *J. Chem. Phys.* **2009**, *130*, 164115.

(33) Beran, G. J. O.; Nanda, K. *J. Phys. Chem. Lett.* **2010**, *1*, 3480–3487.

(34) Wen, S.; Beran, G. J. O. *J. Chem. Theory Comput.* **2011**, *7*, 3733–3742.

(35) Nanda, K.; Beran, G. J. O. *J. Chem. Phys.* **2012**, *137*, 174106.

(36) Taylor, M. B.; Barrera, G. D.; Allan, N. L.; Barron, T. H. K. *Physical Review B* **1997**, *56*, 14380–14390.

(37) Otero-de-la Roza, A.; Johnson, E. R. *J. Chem. Phys.* **2012**, *137*, 054103.

(38) Carrier, P.; Wentzcovitch, R.; Tsuchiya, J. *Phys. Rev. B* **2007**, *76*, 064116.

(39) Day, G. M.; Price, S. L. *J. Am. Chem. Soc.* **2003**, *125*, 16434–43.

(40) Gray, A. E.; Day, G. M.; Leslie, M.; Price, S. L. *Mol. Phys.* **2004**, *102*, 1067–1083.

(41) Filippini, G.; Gramaccioli, C. M.; Simonetta, M.; Suffritti, G. B. *Chem. Phys. Lett.* **1975**, *35*, 17–20.

(42) Filippini, G.; Gramaccioli, C. M. *Acta Cryst. A* **1981**, *37*, 335–342.

(43) Ramírez, R.; Neuerburg, N.; Herrero, C. P. *J. Chem. Phys.* **2012**, *134503*, 134503.

(44) Ramírez, R.; Neuerburg, N.; Herrero, C. P. *J. Chem. Phys.* **2012**, *137*, 044502.

(45) Pamuk, B.; Soler, J. M.; Ramírez, R.; Herrero, C. P.; Stephens, P. W.; Allen, P. B.; Fernández-Serra, M.-V. *Phys. Rev. Lett.* **2012**, *108*, 193003.

(46) Born, M.; Huang, K. *Dynamical Theory of Crystal Lattices*; Clarendon Press, 1954.

(47) Hirata, S. *J. Chem. Phys.* **2008**, *129*, 204104.

(48) Pauling, L. *J. Am. Chem. Soc.* **1935**, *57*, 2680–2684.

(49) Nahringbauer, I. *Acta Chem. Scand.* **1970**, *24*, 453.

(50) McMullan, R. K.; Epstein, J.; John, R.; Craven, B. M. *Acta Cryst. B* **1979**, *35*, 688–691.

(51) Morrison, I.; Li, J. C.; Jenkin, S.; Xantheas, S. S.; Payne, M. C. *J. Phys. Chem. B,* **1997**, *101*, 6146.

(52) Heit, Y.; Beran, G. J. O. *J. Comp. Chem.* **2014**, *35*, 2205–2214.

(53) Boys, S. F.; Bernardi, F. *Mol. Phys.* **1970**, *19*, 553–566.

(54) Dunlap, B. I. *J. Chem. Phys.* **1983**, *78*, 3140–3142.

(55) Weigend, F.; Häser, M.; Patzelt, H.; Ahlrichs, R. *Chem. Phys. Lett.* **1998**, *294*, 143–152.

(56) Feyereisen, M. W.; Fitzgerald, G.; Komornicki, A. *Chem. Phys. Lett.* **1993**, *208*, 359–363.

(57) Weigend, F. *Phys. Chem. Chem. Phys.* **2002**, *4*, 4285–4291.

(58) Dunning, T. H. *J. Chem. Phys.* **1989**, *90*, 1007–1023.

(59) Weigend, F.; Köhn, A.; Hättig, C. *J. Chem. Phys.* **2002**, *116*, 3175–3183.

(60) MOLPRO, version 2012.1, a package of ab initio programs, H.-J. Werner, P. J. Knowles, G. Knizia, F. R. Manby, M. Schütz, P. Celani, T. Korona, R. Lindh, A. Mitrushenkov, G. Rauhut, K. R. Shamasundar, T. B. Adler, R. D. Amos, A. Bernhardsson, A. Berning, D. L. Cooper, M. J. O. Deegan, A. J. Dobbyn, F. Eckert, E. Goll, C. Hampel, A. Hesselmann, G. Hetzer, T. Hrenar, G. Jansen, C. Köppl, Y.

Liu, A. W. Lloyd, R. A. Mata, A. J. May, S. J. McNicholas, W. Meyer, M. E. Mura, A. Nicklass, D. P. O'Neill, P. Palmieri, D. Peng, K. Pflüger, R. Pitzer, M. Reiher, T. Shiozaki, H. Stoll, A. J. Stone, R. Tarroni, T. Thorsteinsson, and M. Wang, see http://www.molpro.net.

(61) Werner, H.-J.; Knowles, P. J.; Knizia, G.; Manby, F. R.; Schütz, M. *WIREs Comput. Mol. Sci.* **2012**, *2*, 242–253.

(62) Karton, A.; Martin, J. M. L. *Theor. Chem. Acc.* **2006**, *115*, 330–333.

(63) Helgaker, T.; Klopper, W.; Koch, H.; Noga, J. *J. Chem. Phys.* **1997**, *106*, 9639–9646.

(64) Ren, P.; Ponder, J. W. *J. Phys. Chem. B* **2003**, *107*, 5933–5947.

(65) Ponder, J. W.; Wu, C.; Ren, P.; Pande, V. S.; Chodera, J. D.; Schnieders, M. J.; Haque, I.; Mobley, D. L.; Lambrecht, D. S.; DiStasio, R. A.; Head-Gordon, M.; Clark, G. N. I.; Johnson, M. E.; Head-Gordon, T. *J. Phys. Chem. B* **2010**, *114*, 2549–64.

(66) J. W. Ponder, TINKER v6.3, 2014, `http://dasher.wustl.edu/tinker/`; Accessed August 10, 2015.

(67) Wu, J. C.; Chattree, G.; Ren, P. *Theor. Chem. Acc.* **2012**, *131*, 1138.

(68) Sebetci, A.; Beran, G. J. O. *J. Chem. Theory Comput.* **2010**, *6*, 155–167.

(69) Stone, A. J. *The Theory of Intermolecular Forces*; Clarendon Press: Oxford, 2002.

(70) A. J. Misquitta and A. J. Stone, CamCASP v5.6 (2011), `http://www-stone.ch.cam.ac.uk/programs.html`. Accessed Februrary 23, 2011.

(71) Kästner, J.; Carr, J. M.; Keal, T. W.; Thiel, W.; Wander, A.; Sherwood, P. *J. Phys. Chem. A* **2009**, *113*, 11856–11865.

(72) Hermann, A.; Schwerdtfeger, P. *Phys. Rev. Lett.* **2008**, *101*, 183005.

(73) Acree, W.; Chickos, J. S. *J. Phys. Chem. Ref. Data* **2010**, *39*, 043101.

(74) Krupskii, I. N.; Prokhvatilov, A.; Erenburg, A. I.; Barylnik, A. S. *Fiz. Nizk. Temp.* **1982**, *8*, 533.

(75) Petrenko, V. F.; Whitworth, R. W. *Physics of Ice*; Oxford University Press, 1999.

(76) Boese, R.; D, B.; Latz, R.; Bäumen, A. *Acta Cryst. C* **1999**, *C55*, 9900001.

(77) Jönson, P. *Acta Cryst.* **1971**, *B27*, 893–898.

(78) Craven, B. M.; McMullan, R. K.; Bell, J. D.; Freeman, H. C. *Acta Cryst. B* **1977**, *B33*, 2585.

(79) Deschamps, J. R.; Cook, J. M.; Teng, Y. *Private Communication* **2008**,

(80) Epstein, J.; Ruble, J. R.; Craven, B. M. *Acta Cryst. B* **1982**, *38*, 140.

(81) Will, G. *Z.Kristallogr.,Kristallgeom.,Kristallphys.,Kristallchem.* **1969**, *129*, 211.

(82) Yu, K.; Schmidt, J. R. *J. Chem. Phys.* **2012**, *136*, 034503.

(83) Babin, V.; Medders, G. R.; Paesani, F. *J. Chem. Theory Comput.* **2014**, *10*, 1599–1607.

(84) Medders, G. R.; Götz, A. W.; Morales, M. A.; Bajaj, P.; Paesani, F.; Medders, G. R.; Götz, A. W.; Morales, M. A.; Bajaj, P.; Paesani, F. *J. Chem. Phys.* **2015**, *143*, 104102.

(85) Sinnokrot, M. O.; Sherrill, C. D. *J. Phys. Chem. A* **2006**, *110*, 10656–10668.

(86) Riley, K. E.; Pitonak, M.; Jurecka, P.; Hobza, P. *Chem. Rev.* **2010**, *110*, 5023–63.

(87) Hesselmann, A. *J. Chem. Phys.* **2008**, *128*, 144112.

(88) Pitonak, M.; Hesselmann, A. *J. Chem. Theory Comput.* **2010**, *6*, 168–178.

(89) Grimme, S. *WIRES: Comput. Mol. Sci.* **2011**, *1*, 211–228.

(90) Kronik, L.; Tkatchenko, A. *Acc. Chem. Res.* **2014**, *47*, 3208–3216.

(91) Berland, K.; Cooper, V. R.; Lee, K.; Schröder, E.; Thonhauser, T.; Hyldgaard, P.; Lundqvist, B. I. *Rep. Prog. Phys.* **2015**, *78*, 066501.

(92) Beyer, T.; Price, S. L. *CrystEngComm* **2000**, *2*, 183.

(93) Gavezzotti, A. *J. Am Chem. Soc.* **2000**, *122*, 10724–10725.

(94) Beran, G. J. O. *Chem. Rev.* **2016**, submitted.

(95) Giauque, W. F.; Egan, C. *J. Chem. Phys.* **1937**, *5*, 45.

(96) Azreg-Aïnou, M. *Montsh. Chem.* **2005**, *136*, 2017.

(97) Giauque, W. F.; Egan, C. J. *J. Chem. Phys.* **1937**, *5*, 45.

(98) Herzberg, G. *Electronic Spectra and Electronic Structure of Polyatomic Molecules*; D. Van Nostrand Company, Inc, 1966.

(99) Shimanouchi, T. *Tables of Molecular Vibrational Frequencies*; NSRDS NBS-39; United States Department of Commerce, 1972; Vol. 1.

(100) Feistel, R.; Wagner, W. *Geochim. Cosmochim. Acta* **2007**, *71*, 36–45.

(101) NIST/TRC Web Thermo Tables (WTT), NIST Standard Reference Subscription Database 2—Lite Edition Version 2-2012-1-Lite.

(102) Haynes, W. M., Ed. *Handbook of Chemistry and Physics*, 96th ed.; CRC Press, 2004.

(103) Feistel, R.; Wagner, W. *J. Phys. Chem. Ref. Data* **2006**, *35*, 1021–1047.

(104) Verevkin, S. *J. Chem. Eng. Data* **2000**, *45*, 953.

(105) Martin, J.; Andon, R. L. *J. Chem. Thermo.* **1982**, *14*, 679.

(106) Jiménez, P.; M.V. Roux, C. T. *J. Chem. Thermo.* **1987**, *19*, 985.

(107) De Wit, H. G. M.; De Kruif, C. G.; Van Miltenburg, J. C. *J. Chem. Thermo.* **1983**, *15*, 891.

(108) Billes, F.; Endrédi, H.; Jalsovszky, G. *J. Mol. Struct. (Theochem)* **1999**, *465*, 157.